

1 High-level cognition is supported by information-rich but
2 compressible brain activity patterns

3 Lucy L. W. Owen^{1,2} and Jeremy R. Manning^{1,*}

¹Department of Psychological and Brain Sciences,
Dartmouth College, Hanover, NH

²Carney Institute for Brain Sciences,
Brown University, Providence, RI

*Address correspondence to jeremy.r.manning@dartmouth.edu

4 December 21, 2023

5 **Abstract**

6 Brain activity patterns are highly flexible and often complex, but also highly structured.
7 Here we examined how fundamental properties of brain activity patterns relate to ongoing
8 cognitive processes. To this end, we applied dimensionality reduction algorithms and pattern
9 classifiers to functional neuroimaging data collected as participants listened to a story, tem-
10 porally scrambled versions of the story, or underwent a resting state scanning session. These
11 experimental conditions were intended to require different depths of processing and inspire
12 different levels of cognitive engagement. We considered two primary aspects of the data. First,
13 we treated the maximum achievable decoding accuracy across participants as an indicator of
14 the “informativeness” of the recorded patterns. Second, we treated the number of features
15 (components) required to achieve a threshold decoding accuracy as a proxy for the “compress-
16 ability” of the neural patterns (where fewer components indicate greater compression). Overall,
17 we found that the peak decoding accuracy (achievable without restricting the numbers of fea-
18 tures) was highest in the intact (unscrambled) story listening condition. However, the number
19 of features required to achieve comparable classification accuracy was also lowest in the intact
20 story listening condition. Taken together, our work suggests that our brain networks flexibly
21 reconfigure according to ongoing task demands, and that the activity patterns associated with
22 higher-order cognition and high engagement are both more informative and more compressible
23 than the activity patterns associated with lower-order tasks and lower levels of engagement.

24 **Keywords:** information, compression, temporal decoding, dimensionality reduction, neu-
25 roimaging

26 **Introduction**

27 Large-scale networks, including the human brain, may be conceptualized as occupying one or
28 more positions along on a continuum. At one extreme, every node is fully independent from
29 every other node. At the other extreme, all nodes behave identically. Each extreme optimizes

30 key properties of how the network functions. When every node is independent, the network is
31 maximally *expressive*: if we define the network’s “state” as the activity pattern across its nodes, then
32 every state is equally reachable by a network with fully independent nodes. On the other hand, a
33 network of identically behaved nodes optimizes *robustness*: any subset of nodes may be removed
34 from the network without any loss of function or expressive power, as long as any single node
35 remains. Presumably, most natural systems tend to occupy positions between these extremes. We
36 wondered: might the human brain reconfigure itself to be more flexible or more robust according
37 to ongoing demands? In other words, might the brain reconfigure its connections or behaviors
38 under different circumstances to change its position along this continuum?

39 Closely related to the above notions of expressiveness versus robustness are measures of
40 how much *information* is contained in a given signal or pattern, and how *redundant* a signal
41 is (Shannon, 1948). Formally, information is defined as the amount of uncertainty about a given
42 variables’ outcomes (i.e., entropy), measured in *bits*, or the optimal number of yes/no questions
43 needed to reduce uncertainty about the variable’s outcomes to zero. Highly complex systems with
44 many degrees of freedom (i.e., high flexibility and expressiveness), are more information-rich than
45 simpler or more constrained systems. The redundancy of a signal denotes the difference between
46 how expressive the signal *could* be (i.e., proportional to the number of unique states or symbols
47 used to transmit the signal) and the actual information rate (i.e., the entropy of each individual
48 state or symbol). If a brain network’s nodes are fully independent, then the number of bits required
49 to express a single activity pattern is proportional to the number of nodes. The network would
50 also be minimally redundant, since the status of every node would be needed to fully express a
51 single brain activity pattern. If a brain network’s nodes are fully coupled and identical, then the
52 number of bits required to express a single activity pattern is proportional to the number of unique
53 states or values any individual node can take on. Such a network would be highly redundant,
54 since knowing any individual node’s state would be sufficient to recover the full-brain activity
55 pattern. Highly redundant systems are also robust, since there is little total information loss due
56 to removing any given observation.

57 We take as a given that brain activity is highly flexible: our brains can exhibit nearly infinite
58 varieties of activity patterns. This flexibility implies that our brains’ activity patterns are highly
59 information rich. However, brain activity patterns are also highly structured. For example,

60 full-brain correlation matrices are stable within (Finn et al., 2017, 2015; Gratton et al., 2018) and
61 across (Cole et al., 2014; Glerean et al., 2012; Gratton et al., 2018; Yeo et al., 2011) individuals. This
62 stability suggests that our brains' activity patterns are at least partially constrained, for example
63 by anatomical, external, or internal factors. Constraints on brain activity that limit its flexibility
64 decrease expressiveness (i.e., its information rate). However, constraints on brain activity also
65 increase its robustness to noise (e.g., "missing" or corrupted signals may be partially recovered).
66 For example, recent work has shown that full-brain activity patterns may be reliably recovered
67 from only a relatively small number of implanted electrodes (Owen et al., 2020; Scangos et al.,
68 2021). This robustness property suggests that the relevant signal (e.g., underlying factors that
69 have some influence over brain activity patterns) are compressible.

70 To the extent that brain activity patterns contain rich task-relevant information, we should be
71 able to use the activity patterns to accurately differentiate between different aspects of a task (e.g.,
72 using pattern classifiers; Norman et al., 2006). For example, prior work has shown a direct
73 correspondence between classification accuracy and the information content of a signal (Alvarez,
74 2002). To the extent that brain activity patterns are compressible, we should be able to generate
75 simplified (e.g., lower dimensional) representations of the data while still preserving the relevant
76 or important aspects of the original signal. In general, information content and compressibility
77 are often related but are also dissociable (Fig. 1). If a given signal (e.g., a representation of brain
78 activity patterns) contains more information about ongoing cognitive processes, then the peak
79 decoding accuracy should be high. In the simulations shown in Figure 1C we construct synthetic
80 datasets that have high or low levels of informativeness by varying temporal autocorrelations
81 in the data (see *Synthetic data*). If a signal is compressible, then a low-dimensional embedding
82 of the signal will be similarly informative as the original signal. In the simulations shown in
83 Figure 1C we construct synthetic datasets that have high or low levels of compressibility by
84 varying the covariance structure across features (see *Synthetic data*). As shown in Figure 1D, highly
85 informative datasets yield higher decoding accuracies than less informative datasets (i.e., the peaks
86 of the curves in the top panels of Fig. 1D are higher than the peaks of the curves in the bottom
87 panels). Highly compressible datasets show steeper slopes when we plot decoding accuracy as a
88 function of the number of components used to represent the data (i.e., the slopes of the curves in
89 the left panels of Fig. 1D are steeper than the slopes of the curves in the right panels). Whereas

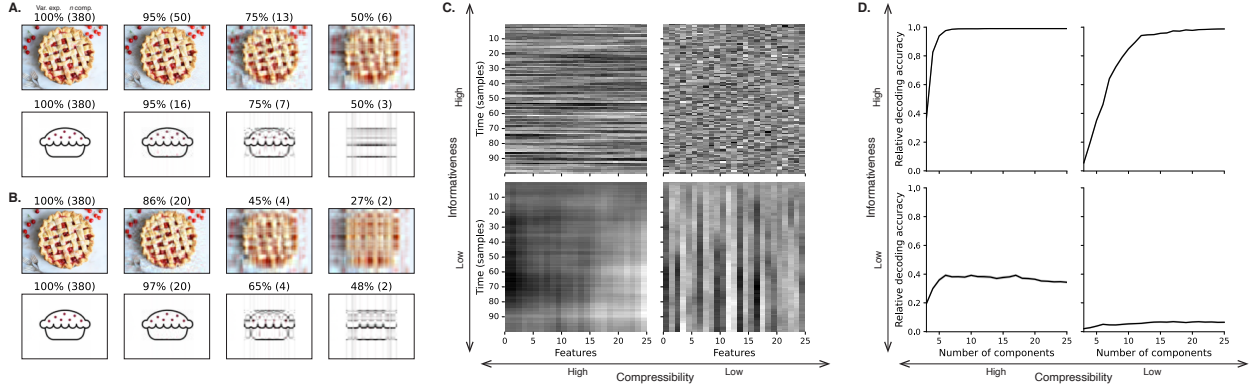


Figure 1: Information content and compressibility. **A. Variance explained for two images.** Consider two example images: a photograph and simple drawing. The images have the same resolutions, but their content is very different. The photograph is more information rich: when we compare the original photograph and drawing (leftmost column), we can see that the photograph captures much more detail. We can also apply principal components analysis to the images, treating the rows of the images as “observations.” Across columns, we identified the numbers of components required to explain 100%, 95%, 75%, or 50% of the cumulative variance in each image (the 100% columns denote the original images). The numbers of components are indicated in parentheses, and the resulting “compressed” images are displayed. This analysis reveals that the drawing is more compressible: just 16 components can explain 95% of the variance in the drawing, whereas 50 components are required to explain 95% of the variance in the photograph. **B. Representing two images with different numbers of components.** Using the same principal component decompositions as in Panel A, we computed the cumulative proportion of variance explained with 380 (original images), 20, 4, or 2 components. This analysis provides another way of characterizing the compressibility of each image by showing that the same number of components can explain more variance in the drawing than in the photograph. **C. Template data from four synthetic datasets.** We constructed four synthetic datasets, each comprising 25 features (columns) observed across 100 samples (rows) from each of 10 simulated “participants.” The datasets were constructed to contain different levels of informativeness and compressibility (see *Synthetic data*). **D. Decoding accuracy by number of components.** For each synthetic dataset, we trained across-participant classifiers to decode timepoint labels. Each panel displays the decoding accuracy as a function of the number of components used to represent the data. Error ribbons denote bootstrap-estimated 95% confidence intervals.

90 characterizing the informativeness and compressibility of synthetic data can be instructive, we
91 are ultimately interested in understanding how these properties relate to brain activity patterns
92 recorded under different cognitive circumstances.

93 Several recent studies suggest that the complexity of brain activity is task-dependent, whereby
94 simpler tasks with lower cognitive demands are reflected by simpler and more compressible brain
95 activity patterns, and more complex tasks with higher cognitive demands are reflected by more
96 complex and less compressible brain activity patterns (Mack et al., 2020; Owen et al., 2021). These
97 findings complement other work suggesting that functional connectivity (correlation) patterns are
98 task-dependent (Cole et al., 2014; Finn et al., 2017; Owen et al., 2020), although see Gratton et
99 al. (2018). Higher-order cognitive processing of a common stimulus also appears to drive more
100 stereotyped task-related activity and functional connectivity across individuals (Hasson et al.,
101 2008; Lerner et al., 2011; Simony & Chang, 2020; Simony et al., 2016).

102 The above studies are consistent with two potential descriptions of how cognitive processes are
103 reflected in brain activity patterns. One possibility is that the information rate of brain activity in-
104 creases during more complex or higher-level cognitive processing. If so, then the ability to reliably
105 decode cognitive states from brain activity patterns should improve with task complexity or with
106 the level (or “depth”) of cognitive processing. A second possibility is that the compressibility of
107 brain activity patterns increases during more complex or higher-level cognitive processing. If so,
108 then individual features of brain recordings, or compressed representations of brain recordings,
109 should carry more information during complex or high-level (versus simple or low-level) cognitive
110 tasks.

111 We used a previously collected neuroimaging dataset to estimate the extent to which each of
112 these two possibilities might hold. The dataset we examined comprised functional magnetic reso-
113 nance imaging (fMRI) data collected as participants listened to an audio recording of a 10-minute
114 story, temporally scrambled recordings of the story, or underwent a resting state scan (Simony
115 et al., 2016). Each of these experimental conditions evokes different depths of cognitive process-
116 ing (Hasson et al., 2008; Lerner et al., 2011; Owen et al., 2021; Simony et al., 2016). We used
117 across-participant classifiers to decode listening times in each condition, as a proxy for how “infor-
118 mative” the task-specific activity patterns were (Simony & Chang, 2020). We also used principle
119 components analysis to generate lower-dimensional representations of the activity patterns. We

120 then repeated the classification analyses after preserving different numbers of components and
121 examined how classification accuracy changed across the different experimental conditions.

122 Results

123 We sought to understand whether higher-level cognition is reflected by more reliable and in-
124 formative brain activity patterns, and how compressibility of brain activity patterns relates to
125 cognitive complexity. We developed a computational framework for systematically assessing the
126 informativeness and compressibility of brain activity patterns recorded under different cognitive
127 circumstances. We used across-participant decoding accuracy (see *Forward inference and decoding*
128 *accuracy*) as a proxy for informativeness. To estimate the compressibility of the brain patterns, we
129 used group principal components analysis (PCA) to project the brain patterns into k -dimensional
130 spaces, for different values of k (see *Hierarchical Topographic Factor Analysis (HTFA)* and *Principal*
131 *components analysis (PCA)*). For more compressible brain patterns, decoding accuracy should be
132 more robust to small values of k .

133 We analyzed a dataset collected by Simony et al. (2016) that comprised four experimental con-
134 ditions. These conditions exposed participants to stimuli that systematically varied in cognitive
135 engagement. In the *intact* experimental condition, participants listened to an audio recording of a
136 10-minute Moth Radio Hour story, *Pie Man*, by Jim O’Grady. In the *paragraph*-scrambled experi-
137 mental condition, participants listened to a temporally scrambled version of the story, where the
138 paragraphs occurred out of order, but where the same set of paragraphs was presented over the
139 entire listening interval. All participants in this condition experienced the scrambled paragraphs
140 in the same order. In the *word*-scrambled experimental condition, participants listened to a tem-
141 porally scrambled version of the story, where the words occurred in a random order. Again, all
142 participants in this condition experienced the scrambled words in the same order. Finally, in the
143 *rest* experimental condition, participants lay in the scanner with no overt stimulus, while keeping
144 their eyes open and blinking as needed. This public dataset provided a convenient means for
145 testing our hypothesis that different levels of cognitive processing and engagement affect how
146 informative and compressible the associated brain patterns are.

147 To evaluate the relation between informativeness and compressibility for brain activity from

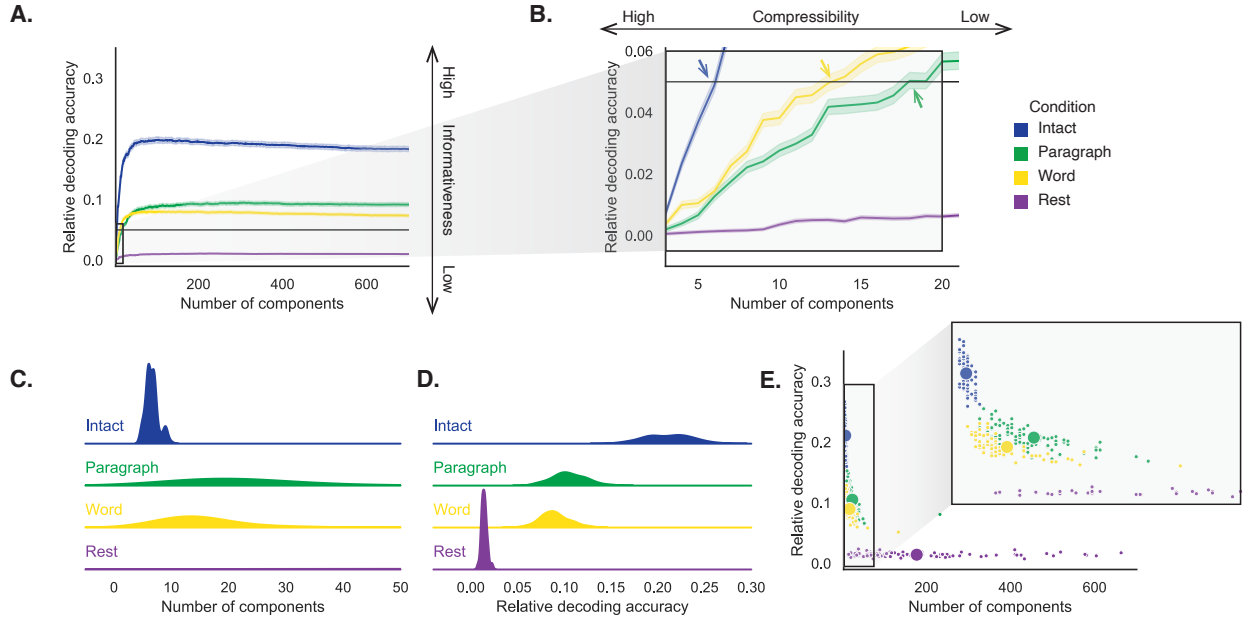


Figure 2: Decoding accuracy and compression. A. Decoding accuracy by number of components. Ribbons of each color display cross-validated decoding performance for each condition (intact, paragraph, word, and rest), as a function of the number of components (features) used to represent the data. For each condition, decoding accuracy has been normalized by subtracting expected “chance” decoding performance (estimated as $\frac{1}{T}$, where T is the number of timepoints in the given condition). This normalization was intended to enable fairer comparisons across conditions; a relative decoding accuracy of 0.0 denotes “chance” performance. The horizontal black line denotes 5% decoding accuracy (used as a reference in Panel B). **B. Numbers of components required to reach a fixed decoding accuracy threshold, by condition.** The panel displays a zoomed-in view of the inset in Panel A. Intersections between each condition’s decoding accuracy curve and the 5% decoding accuracy reference line are marked by arrows. All error ribbons in Panels A and B denote bootstrap-estimated 95% confidence intervals. **C. Estimating “compressibility” for each condition.** The density plots display the numbers of components required to reach at least 5% (corrected) decoding accuracy, across all cross validation runs. For the “rest” condition, where decoding accuracy never reached 5% accuracy, we display the distribution of the numbers of components required to achieve the peak decoding accuracy in each fold. (This distribution is nearly flat, as also illustrated in Panel E.) **D. Estimating “informativeness” for each condition.** The density plots display the peak (corrected) decoding accuracies achieved in each condition, across all cross validation runs. **E. Informativeness versus compressibility.** Each dot displays the minimum number of components required to achieve at least 5% corrected decoding accuracy (x -coordinate; for the rest condition the numbers of components are estimated using the peak decoding accuracies as in Panel C) and the peak (corrected) decoding accuracy (y -coordinate). The smaller dots correspond to individual cross validation runs and the larger dots display the averages across runs. The inset displays a zoomed-in view of the indicated region in the main panel.

148 each experimental condition, we trained a series of across-participant temporal decoders on com-
149 pressed representations of the data. Figure 2A displays the decoding accuracy as a function
150 of the number of principal components used to represent the data (also see Fig. S1). Several
151 patterns were revealed by the analysis. First, in general (i.e., across experimental conditions),
152 decoding accuracy tends to improve as the number of components are increased. However, de-
153 coding accuracy peaked at higher levels for experimental conditions that exposed participants
154 to cognitively richer stimuli (Fig. 2D). The peak decoding accuracy was highest for the “intact”
155 condition (versus paragraph: $t(99) = 35.205, p < 0.001$; versus word: $t(99) = 43.172, p < 0.001$);
156 versus rest: $t(99) = 81.361, p < 0.001$), next highest for the “paragraph” condition (versus word:
157 $t(99) = 6.243, p < 0.001$; versus rest: $t(99) = 50.748, p < 0.001$), and next highest for the “word”
158 condition (versus rest: $t(99) = 48.791, p < 0.001$). This ordering implies that cognitively richer
159 conditions evoke more stable brain activity patterns across people.

160 The cognitively richer conditions also displayed steeper initial slopes. For example, the intact
161 condition decoders reached an arbitrarily chosen threshold of 5% accuracy using fewer components
162 than the paragraph condition decoders ($t(99) = -7.429, p < 0.001$) or word condition decoders
163 ($t(99) = -7.300, p < 0.001$), and decoding accuracy never exceeded 5% for the rest condition. This
164 suggests that brain activity patterns evoked by cognitively richer conditions are more compressible,
165 such that representing the data using the same number of principal components provides more
166 information to the temporal decoders (Figs. 2B, C). Taken together, as shown in Figure 2E, we
167 found that brain activity patterns evoked by cognitively richer conditions tended to be both more
168 informative (i.e., associated with higher peak decoding accuracies) *and* more compressible (i.e.,
169 requiring fewer components to achieve the 5% accuracy threshold).

170 If informativeness (to the temporal decoders) and compressibility vary with the cognitive
171 richness of the stimulus, might these measures also vary over time *within* a given condition? For
172 example, participants in the intact condition might process the ongoing story more deeply later
173 on in the story (compared with earlier in the story) given the additional narrative background
174 and context they had been exposed to by that point. To examine this possibility, we divided each
175 condition into four successive time segments. We computed decoding curves (Fig. 3A) and the
176 numbers of components required to achieve 5% decoding accuracy (Fig. 3B) for each segment and
177 condition. We found that, in the two most cognitively rich conditions (intact and paragraph), both

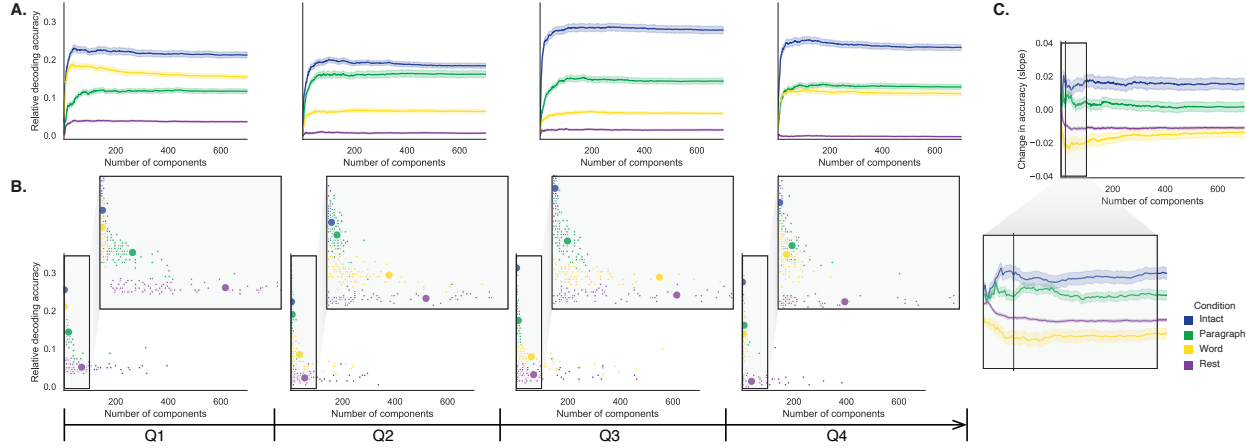


Figure 3: Changes in decoding accuracy and compression over time. **A. Decoding accuracy by number of components, by story segment.** Each family of curves is plotted in the same format as Figure 2A but reflects data only from one quarter of the dataset. **B. Informativeness versus compressibility by condition and segment.** Each scatter plot is in the same format as Figure 2E, but reflects data only from one quarter of the dataset. **C. Change in decoding accuracy over time, by number of components.** For each number of components (x -axis) and condition (color), we fit a regression line to the decoding accuracies obtained for the first, second, third, and fourth quarters of the dataset (corresponding to the columns of Panels A and B). The y -axis denotes the slopes of the regression lines. The black vertical line marks $k = 20$ components, as referenced in the main text. All error ribbons denote bootstrap-estimated 95% confidence intervals.

178 decoding accuracy and compressibility, as reflected by the change in decoding curves, increased
 179 with listening time (e.g., at the annotated reference point of $k = 20$ components in Fig. 3C: intact:
 180 $t(99) = 7.915, p < 0.001$; paragraph: $t(99) = 2.354, p = 0.021$). These changes may reflect an increase
 181 in comprehension or depth of processing with listening time. In contrast, the decoding accuracy
 182 and compressibility *decreased* with listening time in the word condition ($t(99) = -10.747, p < 0.001$)
 183 and rest condition ($t(99) = -22.081, p < 0.001$). This might reflect the depletion of attentional
 184 resources in the less-engaging word and rest conditions.

185 These results make some intuitive sense. As the contextual information available to participants
 186 increases (i.e., over time in the cognitively rich intact and paragraph conditions), it makes sense that
 187 this might constrain neural responses to a greater extent. While this pattern may not necessarily
 188 hold for *every* possible story or stimulus, we suspect that it is generally the case that our knowledge
 189 about what is happening in a story tends to increase as we experience more about it. In turn, this
 190 could lead to greater consistency in different people’s interpretations of and neural responses to
 191 the stimulus. Similarly, as participants are left to “mind wander,” or as they experience mental

192 fatigue (i.e., over time in the less cognitively rich word and rest conditions), we suggest that this
193 might lead to greater variability in neural responses across people, resulting in lower decoding
194 accuracy. Again, it is not necessarily the case that every possible “unengaging” stimulus will
195 lead to greater neural variability as time progresses, but we suspect this phenomenon is likely to
196 hold for a variety of such stimuli. These findings replicate at least to a limited extent (e.g., across
197 both cognitively rich conditions and across both cognitively impoverished conditions, and for the
198 different groups of participants in each of those conditions). However, determining whether these
199 patterns generalize to other stimuli would require additional study (with new stimuli).

200 If the informativeness and compressibility of brain activity patterns vary over time, do these
201 properties might also vary across brain networks? We used a network parcellation identified by Yeo
202 et al. (2011) to segment the brain into seven distinct networks. The networks can be sorted (roughly)
203 in order from lower-level to higher-level cortex as follows (Figs. 4A–C): visual, somatomotor,
204 dorsal attention, ventral attention, limbic, frontoparietal, and default mode. Next, we computed
205 decoding curves separately for the activity patterns within each network and identified each
206 network’s inflection point, for each experimental condition. Moving from low-order networks
207 to higher-order networks, we found that decoding accuracy tended to increase in the higher-
208 level experimental conditions and decrease (slightly) in the lower-level experimental conditions
209 (Fig. 4D, E; Spearman’s rank correlation between decoding accuracy and network order: intact:
210 $\rho = 0.362, p < 0.001$; paragraph: $\rho = 0.441, p < 0.001$; word: $\rho = -0.102, p = 0.007$; rest: $\rho =$
211 $-0.354, p < 0.001$). This suggests that higher-order networks may carry more content-relevant
212 or stimulus-driven “information.” We found no clear trends in the proportions of components
213 required to achieve 5% decoding accuracy across networks or conditions (Fig. 4F).

214 Whereas the above analyses examine different networks in isolation, how does full-brain
215 (i.e., potentially multi-network) activity patterns reflected by different principal components vary
216 across different experimental conditions? As shown in Figure 5, we used Neurosynth (Rubin et al.,
217 2017) to identify, for each component, the associations with each of 80 themes (see *Reverse inference*).
218 In general, the first principal components across all of the experimental conditions tended to weight
219 most heavily on themes related to cognitive control, memory, language processing, attention, and
220 perception. Other components appeared to vary more across conditions.

221 To gain further insights into which brain functions might be most closely associated with

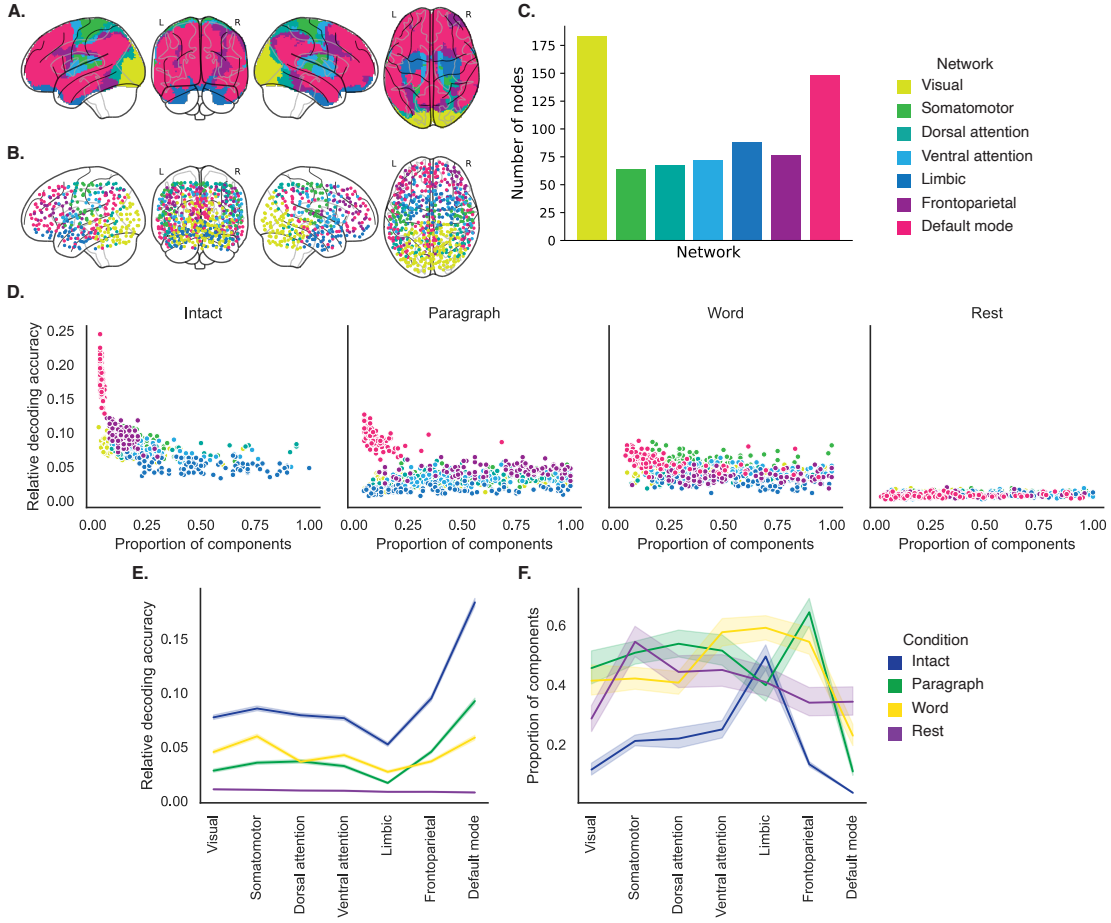


Figure 4: Network-specific decoding accuracy and compression. **A. Network parcellation map.** The glass brain displays the location of each of seven networks identified by Yeo et al. (2011). **B. Node labels.** We assigned network labels to each of 700 Hierarchical Topographic Factor Analysis-derived nodes (see *Hierarchical topographic factor analysis (HTFA)*). For each node, we evaluated its radial basis function (RBF) at the locations of every voxel in the parcellation map displayed in Panel A. We summed up these RBF weights separately for the voxels in each network. We defined each node's network label as its highest-weighted network across all voxels. **C. Per-network node counts.** The bar plot displays the total number of HTFA-derived nodes assigned to each network. **D. Informativeness versus compressibility by network and condition.** Each dot corresponds to a single cross validation run. The dots' coordinates denote the minimum proportion of components (relative to the number of nodes in the given network) required to achieve at least 5% corrected decoding accuracy (x -coordinate; for the rest condition these proportions are estimated using the peak decoding accuracies) and peak (corrected) decoding accuracy (y -coordinate). We repeated the analysis separately for each network (color) and experimental condition (column). **E. Informativeness by network.** For each network, sorted (roughly) from lower-order networks on the left to higher-order networks on the right, the curves display the peak (corrected) decoding accuracy for each experimental condition (color). **F. Compressibility by network.** For each network, the curves display the proportion of components (relative to the total possible number of components displayed in Panel C) required to achieve at least 5% decoding accuracy (or, for the rest condition, peak decoding accuracy, as described above). Error ribbons in Panels E and F denote bootstrap-estimated 95% confidence intervals.

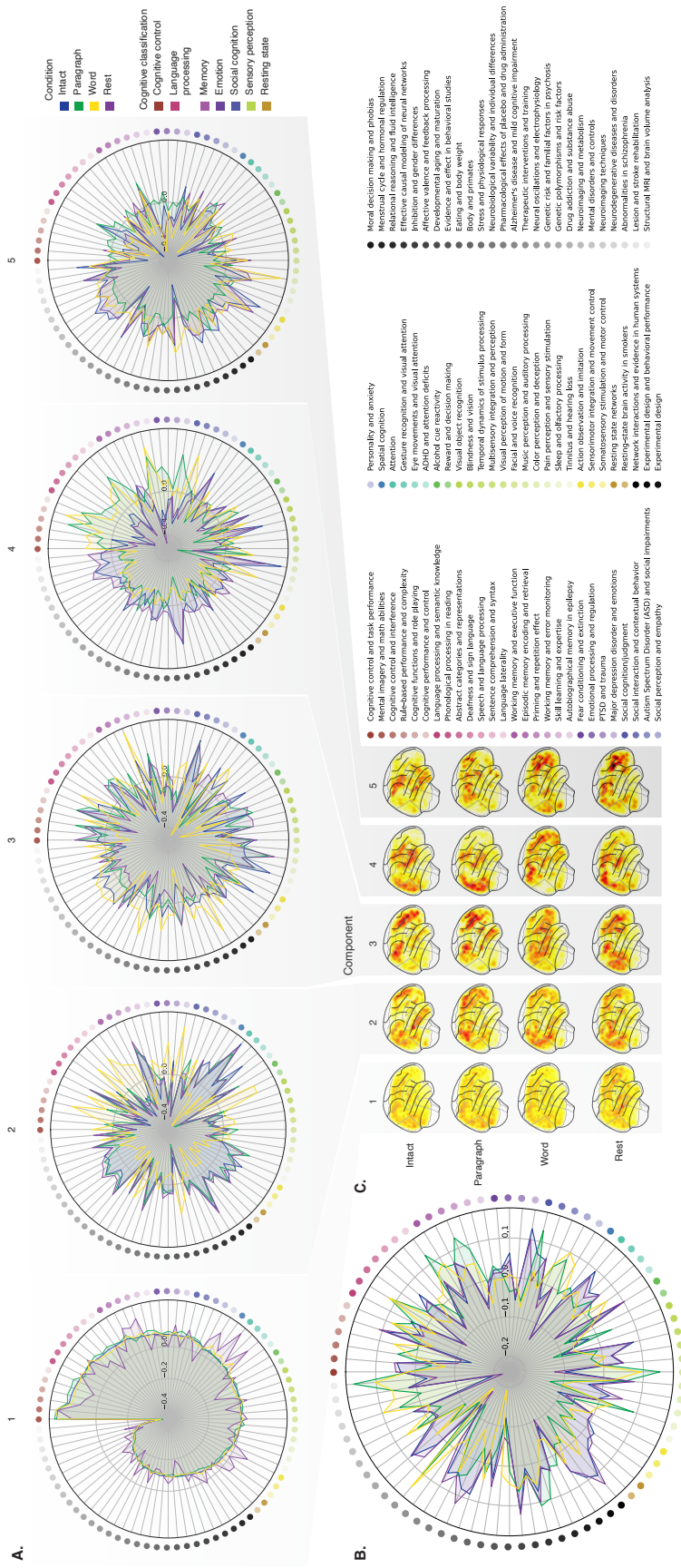


Figure 5: Neurosynth topic weightings by component. We used a reverse inference procedure (see *Reverse inference*) to estimate the correspondences between brain images and a set of 80 topics derived from the Neurosynth database of neuroimaging articles (Rubin et al., 2017). **A. Topic correlations by component.** For each of the top five highest-weighted principal components (columns) derived from each experimental condition (colors), the radar plots display the correlations between the component images and the per-topic images derived for each topic (topic identities are denoted by the blue dots; a legend for the topic labels is in the lower right of the figure). An annotated list of the top-weighted topics for each component and condition may be found in Figure S2 and the top-weighted terms for each topic may be found in Table S1. **B. Topic correlations averaged across components.** The radar plot is in the same format as the plots in Panel A, but here we display the per-condition average correlations across the top five components (for each condition) reflected in Panel A. **C. Component images.** Each plot displays a right sagittal view of a glass brain projection of the top five principal components (columns) for each experimental condition (rows). Additional projections for each component may be found in Figure S3.

the top-weighted components from each experimental condition, we manually grouped each Neurosynth-derived topic into a smaller set of core cognitive functions. Separately for each component, we computed the average weightings across all topics that were tagged as being associated with each of these cognitive functions (Figs. 6A, S5A). To help visualize these associations, we used the patterns of associations for each component to construct graphs whose nodes were experimental conditions and cognitive functions (Figs. 6B, S5B). We also computed correlations between the sets of per-topic weightings from each of the top-weighted components from each experimental condition (Fig. 6C, D) and between the brain maps for each condition's components (Fig. S5C, D). Taken together, we found that each component appeared to weight on a fundamental set of cognitive functions that varied by experimental condition. For example, the top principal components from every condition weighted similarly (across conditions) on the full set of Neurosynth topics (Fig. 5A) and cognitive functions (Figs. 6A, B and S5 A, B), suggesting that these components might reflect a set of functions or activity patterns that are common across all conditions. The second components' weightings were similar across the intact, paragraph, and rest conditions (highest-weighted functions: cognitive control, memory, social cognition, and resting state), but different for the word condition (highest-weighted functions: sensory perception and cognitive control). The fourth components' weighting grouped the paragraph and word conditions (highest-weighted functions: memory, language processing, and cognitive control) and the intact and rest conditions (highest-weighted functions: emotion, social cognition). We also used ChatGPT (OpenAI, 2023) to sort the list of manually tagged cognitive functions from lowest-level to highest-level (Tab. S2, Fig. 6E; also see *Ranking cognitive processes*). We found that higher-level functions tended to be weighted on more heavily by top components from the intact and paragraph conditions than lower-level functions (intact vs. word: $t(198) = 11.059, p < 0.001$; intact vs. rest: $t(198) = 3.699, p < 0.001$; paragraph vs. word: $t(198) = 13.504, p < 0.001$; paragraph vs. rest: $t(198) = 4.812, p < 0.001$; also see *Ranking cognitive processes*). The top components from the word condition showed the opposite tendency, whereby *lower*-level functions tended to be weighted on more heavily than higher-level functions (word vs. rest: $t(198) = -7.315, p < 0.001$). The weighting trends for the intact and paragraph conditions were not reliably different ($t(198) = -0.479, p = 0.633$). The components from the rest condition showed almost no differences in the weights associated with high-level versus low-level functions (rest vs. 0: $t(99) = 1.836, p = 0.081$). These findings suggest that when

252 participants were engaged more strongly (in the more engaging intact and paragraph conditions),
253 their dominant neural patterns reflected higher-level cognitive functions. In contrast, when partic-
254 ipants were engaged less strongly (in the less engaging word and rest conditions), their dominant
255 neural patterns reflected lower-level cognitive functions. Although they were highly statistically
256 reliable, it is also important to note that these latter effects are also relatively small (e.g., the slopes
257 for *all* of the experimental conditions are numerically close to zero; Fig. 6E). We suggest that this
258 phenomenon may merit further investigation in future work.

259 Discussion

260 We examined fMRI data collected as participants listened to an auditory recording of a story, scram-
261 bled recordings of the story, or underwent a resting state scan. We found that cognitively richer
262 stimuli evoked more reliable (i.e., consistent across people) and information rich brain activity pat-
263 terns. The brain patterns evoked by cognitively richer stimuli were also more compressible, in that
264 each individual component provided more “signal” to temporal decoders relative to components
265 of data from less cognitively rich conditions (Fig. 2). Over time (e.g., as the experiment progressed),
266 these phenomena were strengthened. Specifically, across story segments, data from more cogni-
267 tively rich conditions became more informative and compressible, and data from less cognitively
268 rich conditions became *less* informative and compressible (Fig. 3). We also repeated these analyses
269 separately for different brain networks. We found that networks traditionally associated with
270 higher-level cognitive functions tended to provide more informative brain patterns than networks
271 traditionally associated with lower level cognitive functions (Fig. 4). Finally, we examined the most
272 dominant components of the brain activity patterns from each experimental condition. We used a
273 reverse inference approach (Rubin et al., 2017) to identify the terms in the neuroimaging literature
274 most commonly associated with the corresponding maps. As summarized in Figure 6E, we found
275 that the intact and paragraph conditions tended to weight on higher-level cognitive processes
276 more than lower-level cognitive processes, whereas the word condition weighted on lower-level
277 processes more than higher-level processes and the rest condition showed no difference in high-
278 level versus low-level weighting. Taken together, our findings indicate that the informativeness
279 and compressibility of our brain activity patterns are task-dependent, and these properties change

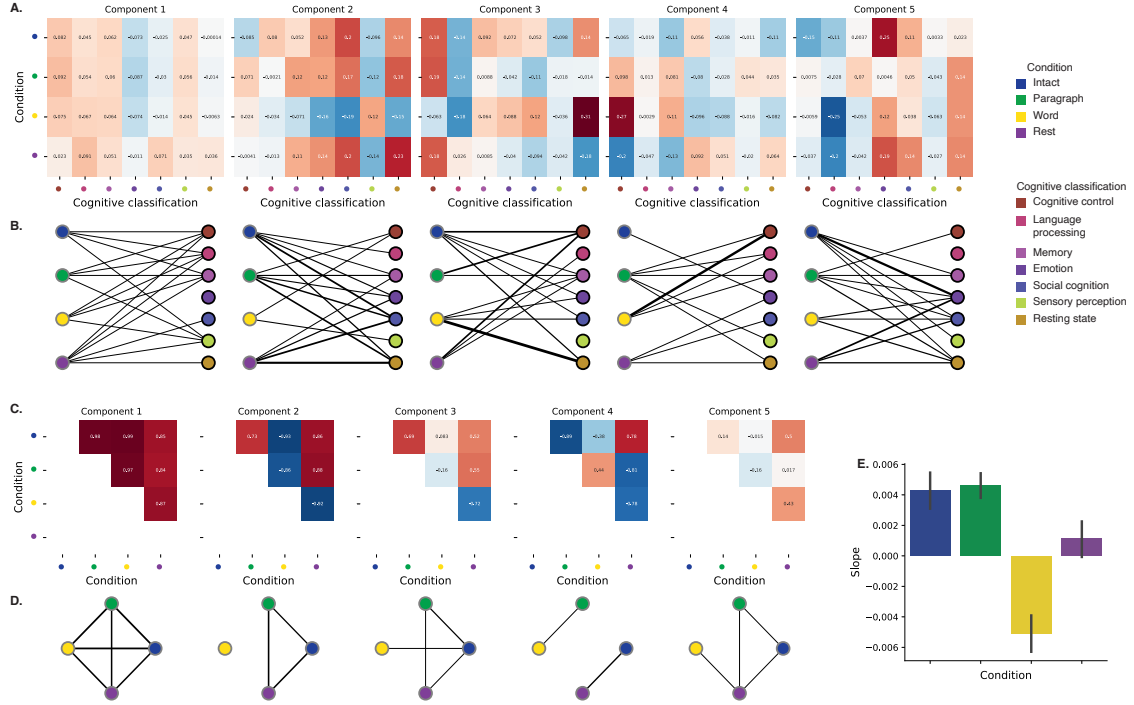


Figure 6: Summary of functions associated with top-weighted components by condition. A. Top-weighted topics by condition. Here we display per-condition (rows, indicated by colored dots) topic correlations, averaged across topics that pertain to each of several broad cognitive functions (columns within each sub-panel, indicated by colored dots). Each sub-panel reflects correlations for the components indicated in the panel titles. A legend for the condition and several core cognitive function classifications is displayed in the lower right of the figure. Table S1 provides a list of each topic’s top-weighted terms, along with each topic’s manually labeled cognitive classification. A full list of the topics most highly associated with each component may be found in Figure S2. **B. Associations between per-condition components and cognitive functions.** The network plots denote positive average correlations between the component images for each condition (gray-outlined dots on the left sides of each network; colors denote conditions) and topic-specific brain maps associated with each indicated cognitive function (black-outlined dots on the right sides of each network; colors denote cognitive functions). The line thicknesses are proportional to the correlation values (correlation coefficients are noted in the heat maps in Panel A). **C. Correlations between each principal component, by condition.** The heat maps display the correlations between the brain maps (Fig. S3) for each principal component (sub-panel), across each pair of conditions (rows and columns of each sub-panel’s matrix, indicated by colored dots). **D. Associations between per-condition components, by component.** Each sub-panel’s network plot summarizes the pattern of correlations between the n^{th} top-weighted principal components (sub-panel) for each experimental condition (gray-outlined dots). The line thicknesses are proportional to the correlation values (correlation coefficients are noted in the heat maps in Panel C). **E. Change in weights by condition.** The bar heights reflect the slopes of regression lines, fit separately to the top five components from each condition, between the ChatGPT-derived “rank” of each cognitive classification and the correlations between the component and topic maps associated with cognitive processes at the given rank (see *Ranking cognitive processes*) Error bars denote bootstrap-estimated 95% confidence intervals. Also see Fig. S5 for additional information.

280 systematically with factors like cognitive richness and depth of processing.

281 Our explorations of informativeness and compressibility are related to a much broader literature
282 on the correlational and causal structure of brain activity patterns and networks (Adachi et
283 al., 2012; Bassett & Sporns, 2017; Brovelli et al., 2004; Bullmore & Sporns, 2009; Dhamala et al.,
284 2008; Korzeniewska et al., 2008; Lynn & Bassett, 2021; Owen et al., 2021; Preti et al., 2017; Rogers
285 et al., 2007; Rubinov & Sporns, 2010; Sizemore et al., 2018; Smith, Beckmann, et al., 2013; Smith,
286 Vidaurre, et al., 2013; Sporns & Betzel, 2016; Sporns & Honey, 2006; Sporns & Zwi, 2004; Srinivasan
287 et al., 2007; Tomasi & Volkow, 2011; Yeo et al., 2011). Correlations or causal associations between
288 different brain regions simultaneously imply that full-brain activity patterns will be compressible
289 and also that those activity patterns will contain redundancies. For example, the extent to which
290 activity patterns at one brain area can be inferred or predicted from activity patterns at other
291 areas (e.g., Owen et al., 2020; Scangos et al., 2021), reflects overlap in the information available
292 in or represented by those brain areas. If brain patterns in one area are recoverable using brain
293 patterns in another area, then a “signal” used to convey the activity patterns could be compressed
294 by removing the recoverable activity. Predictable (and therefore redundant) brain activity patterns
295 are also more robust to signal corruption. For example, even if the activity patterns at one region
296 are unreadable or unreliable at a given moment, that unreliability could be compensated for by
297 other regions’ activity patterns that were predictive of the unreliable region.

298 Our findings that informativeness and compressibility change with task demands may follow
299 from task-dependent changes in full-brain correlation patterns. A number of prior studies have
300 found that so-called “functional connectivity” (i.e., correlational) patterns vary reliably across
301 tasks, events, and situations (Cole et al., 2014; Owen et al., 2021; Simony et al., 2016; Smith et
302 al., 2009). By examining how these task-dependent changes in correlations affect informativeness
303 and compressibility, our work suggests a potential reason why the statistical structure of brain
304 activity patterns might vary with cognitive task or with cognitive demands. For lower-level tasks,
305 or for tasks that require relatively little “deep” cognitive processing, our brains may optimize
306 activity patterns for robustness and redundancy over expressiveness, for example to maximize
307 reliability. For higher-level tasks, or for tasks that require deeper cognitive processing, our brains
308 may sacrifice some redundancy in favor of greater expressiveness.

309 In the information theory sense (Shannon, 1948), when a signal is transmitted using a fixed

310 alphabet of “symbols,” the information rate decreases as the signal is compressed (e.g., fewer sym-
311 bols transmitted per unit time, using an alphabet with fewer symbols, etc.). Our finding that each
312 individual brain component (symbol) becomes more informative as cognitive richness increases
313 suggests that the “alphabet” of brain activity patterns is also task-dependent. Other work suggests
314 that the representations that are *reflected* by brain activity patterns may also change with task de-
315 mands. For example, our brains may represent the same perceptual stimulus differently depending
316 on which aspects of the stimulus or which combinations of features are task-relevant (Mack et al.,
317 2020).

318 Different brain networks also varied in how informative and compressible their activity pat-
319 terns were across experimental conditions (e.g., Fig. 4). This might follow from evolutionary
320 optimizations that reflect the relevant constraints or demands placed on those networks. One
321 possibility is that cortex is organized in a hierarchy of networks “concerned with” or selective to
322 different levels of processing or function. To the extent that different levels of processing (e.g.,
323 low-level sensory processing versus “deeper” higher-level processing) reflect different stimulus
324 timescales (e.g., Manning, 2020), the network differences we observed might also relate to the
325 timescales at which each network is maximally sensitive (Baldassano et al., 2017; Hasson et al.,
326 2008; Lerner et al., 2011; Regev et al., 2018).

327 **Concluding remarks**

328 Cognitive neuroscientists are still grappling with basic questions about the fundamental “rules”
329 describing how our brains respond, and about how brain activity patterns and the associated
330 underlying cognitive representations and computations are linked. We identified two aspects of
331 brain activity patterns, informativeness and compressibility, that appear to change systematically
332 with task demands and across brain networks. Our work helps to clarify how the “neural code”
333 might be structured, and how the code might vary across tasks and brain areas.

334 **Methods**

335 We measured properties of recorded neuroimaging data under different task conditions that varied
336 systematically in cognitive engagement and depth of processing. We were especially interested in

337 how *informative* and *compressible* the activity patterns were under these different conditions (Fig. 1).

338 Unless otherwise noted, all statistical tests are two-sided, all error bars and error ribbons
339 denote bootstrap-estimated 95% confidence intervals across participants, and all reported *p*-values
340 are corrected for multiple comparisons using the Benjamini-Hochberg procedure (Benjamini &
341 Hochberg, 1995).

342 **Functional neuroimaging data collected during story listening**

343 We examined an fMRI dataset collected by Simony et al. (2016) that the authors have made publicly
344 available at arks.princeton.edu/ark:/88435/dsp015d86p269k. The dataset comprises neuroimaging
345 data collected as participants listened to an audio recording of a story (intact condition; 36 par-
346 ticipants), listened to temporally scrambled recordings of the same story (17 participants in the
347 paragraph-scrambled condition listened to the paragraphs in a randomized order and 36 in the
348 word-scrambled condition listened to the words in a randomized order), or lay resting with their
349 eyes open in the scanner (rest condition; 36 participants). Full neuroimaging details may be found
350 in the original paper for which the data were collected (Simony et al., 2016). Procedures were
351 approved by the Princeton University Committee on Activities Involving Human Subjects, and by
352 the Western Institutional Review Board (Puyallup, WA). All subjects were native English speakers
353 with normal hearing and provided written informed consent.

354 **Hierarchical topographic factor analysis (HTFA)**

355 Following our prior related work, we used HTFA (Manning et al., 2018) to derive a compact
356 representation of the neuroimaging data. In brief, this approach approximates the timeseries
357 of voxel activations (44,415 voxels) using a much smaller number of radial basis function (RBF)
358 nodes (in this case, 700 nodes, as determined by an optimization procedure; Manning et al., 2018).
359 This provides a convenient representation for examining full-brain activity patterns and network
360 dynamics. All of the analyses we carried out on the neuroimaging dataset were performed in
361 this lower-dimensional space. In other words, each participant's data matrix was a number-of-
362 timepoints (*T*) by 700 matrix of HTFA-derived factor weights (where the row and column labels
363 were matched across participants). Code for carrying out HTFA on fMRI data may be found as

³⁶⁴ part of the BrainIAK toolbox (Capota et al., 2017; Kumar et al., 2021), which may be downloaded
³⁶⁵ at brainiak.org.

³⁶⁶ **Principal components analysis (PCA)**

³⁶⁷ We applied group PCA (Smith et al., 2014) separately to the HTFA-derived representations of the
³⁶⁸ data (i.e., factor loadings) from each experimental condition. Specifically, for each condition, we
³⁶⁹ considered the set of all participants' T by 700 factor weight matrices. We used group PCA to project
³⁷⁰ these 700-dimensional matrices into a series of shared k -dimensional spaces, for $k \in \{3, 4, 5, \dots, 700\}$.
³⁷¹ This yielded a set of number-of-participants matrices, each with T rows and k columns.

³⁷² **Temporal decoding**

³⁷³ We sought to identify neural patterns that reflected participants' ongoing cognitive processing of
³⁷⁴ incoming stimulus information. As reviewed by Simony et al. (2016), one way of homing in on
³⁷⁵ these stimulus-driven neural patterns is to compare activity patterns across individuals. In partic-
³⁷⁶ ular, neural patterns will be similar across individuals to the extent that the neural patterns under
³⁷⁷ consideration are stimulus-driven, and to the extent that the corresponding cognitive representa-
³⁷⁸ tions are reflected in similar spatial patterns across people (Simony & Chang, 2020). Following this
³⁷⁹ logic, we used an across-participant temporal decoding test developed by Manning et al. (2018) to
³⁸⁰ assess the degree to which different neural patterns reflected ongoing stimulus-driven cognitive
³⁸¹ processing across people. The approach entails using a subset of the data to train a classifier to
³⁸² decode stimulus timepoints (i.e., moments in the story participants listened to) from neural pat-
³⁸³ terns. We use decoding (forward inference) accuracy on held-out data, from held-out participants,
³⁸⁴ as a proxy for the extent to which the inputted neural patterns reflected stimulus-driven cognitive
³⁸⁵ processing in a similar way across individuals.

³⁸⁶ **Forward inference and decoding accuracy**

³⁸⁷ We used an across-participant correlation-based classifier to decode which stimulus timepoint
³⁸⁸ matched each timepoint's neural pattern. For a given value of k (i.e., number of principal compo-
³⁸⁹ nents), we first used group PCA to project the data from each condition into a shared k -dimensional

space. Next, we divided the participants into two groups: a template group, $\mathcal{G}_{\text{template}}$ (i.e., training data), and a to-be-decoded group, $\mathcal{G}_{\text{decode}}$ (i.e., test data). We averaged the projected data within each group to obtain a single T by k matrix for each group. Next, we correlated the rows of the two averaged matrices to form a T by T decoding matrix, Λ . In this way, the rows of Λ reflected timepoints from the template group, while the columns reflected timepoints from the to-be-decoded group. We used Λ to assign temporal labels to each timepoint (row) from the test group's matrix, using the row of the training group's matrix with which it was most highly correlated. We repeated this decoding procedure, but using $\mathcal{G}_{\text{decode}}$ as the template group and $\mathcal{G}_{\text{template}}$ as the to-be-decoded group. Given the true timepoint labels (for each group), we defined the decoding accuracy as the average proportion of correctly decoded timepoints, across both groups (where chance performance is $\frac{1}{T}$). In Figures 2 and 3 we report the decoding accuracy for each condition and value of k , averaged across $n = 100$ cross validation folds.

402 Reverse inference

403 To help interpret the brain activity patterns we found within the contexts of other studies, we
404 created summary maps of each principal component, for each experimental condition. Each
405 principal component comprises 700 “weights” on each of the HTFA-derived RBF nodes (see
406 *Hierarchical Topographic Factor Analysis*). For each node, we evaluated its RBF at the locations of
407 every voxel in the standard 2 mm MNI152 template brain and multiplied the RBF by the node’s
408 weight. The sum of these weighted RBF activation maps provides a full-brain image, in MNI152
409 space, of the given principal component (Fig. S3).

410 Next, we considered 80 topics estimated using Latent Dirichlet Allocation (Blei et al., 2003)
411 applied to 9,204 functional neuroimaging articles in the Neurosynth database (Rubin et al., 2017).
412 The topics, as well as associated brain maps identified using Neurosynth, were identified and
413 reported in several prior studies (Chen et al., 2020; Fox et al., 2014; Sul et al., 2017). The topic
414 labels for each topic were generated automatically with the following ChatGPT (OpenAI, 2023)
415 prompt: “Please help me come up with intuitive labels for topics I found by fitting a topic model
416 to thousands of neuroscience and psychology articles. I’ll paste in the top 10 highest-weighted
417 words for each topic, and I’d like you to respond with a suggested label. For each topic, please

418 respond with just the topic label and no other formatting or text. Here are the next topic's top
419 words:" followed by a comma-separated list of the given topic's top-weighted words reflected
420 in the Table S1. For some topics, ChatGPT responded with a longer-form response rather than a
421 concise topic label. In these instances, on a case-by-case basis, we used a second follow-up prompt
422 to achieve the given topic's label: "Could you please come up with a more concise label for that
423 topic?". We then manually identified a set of 11 cognitive labels that were intended to encapsulate
424 a representative range of widely studied low-level and high-level cognitive functions. In choosing
425 the set of cognitive labels, we jointly considered each topic's ChatGPT-derived topic label, along
426 with the top-weighted words for the topic. We attempted to generate a concise set of labels that
427 still spanned the full set of cognitive functions reflected across the 80 topics. Topics that appeared
428 unrelated to specific cognitive functions (e.g., topics related to specific methods or clinical themes)
429 are designated with dashes in Table S1.

430 Finally, following an approach used in several prior studies (Chen et al., 2020; Fox et al., 2014;
431 Sul et al., 2017) we treated the correlation between a given component's brain map and each topic's
432 brain map as an approximate measure of how much the component was reflective of the given
433 topic. This resulted in a set of 80 "weights" (correlation coefficients) for each component's brain
434 map, with one weight per Neurosynth-derived topic.

435 **Ranking cognitive processes**

436 We manually identified 11 cognitive labels spanning the set of 80 Neurosynth-derived topics:
437 cognitive control, language processing, memory, emotion, social cognition, spatial cognition, at-
438 tention, reward, sensory perception, motor control, and resting state. We then used ChatGPT
439 to automatically "rank" the processes from high-level to low-level using the following prompt:
440 "Please rank these cognitive processes from highest-level to lowest-level, where higher values
441 indicate higher-order or higher-level processes. Return the result as a csv file with a header row
442 and two columns: 'Cognitive label' and 'Rank'. Here are the processes: cognitive control, lan-
443 guage processing, memory, emotion, social cognition, spatial cognition, attention, reward, sensory
444 perception, motor control, resting state". Table S2 displays the output.

445 In the analysis presented in Figure 6E, we summarize difference in topic weightings across

446 experimental conditions. In particular, we sought to characterize how the dominant neural patterns
447 evoked by each experimental condition weighted on different cognitive functions. For each of the
448 top five principal components from each experimental condition (Fig. 5), we computed the average
449 weightings for each of the 11 manually identified (and ChatGPT-ranked) cognitive labels described
450 above (Tab. S2). We then fit a line separately for each experiment condition (x -values: cognitive
451 rank; y -values: weights). In carrying out this analysis, we used a bootstrap procedure to estimate
452 the variability in the slopes of the regression lines, whereby we repeated this process for each of
453 $n = 100$ iterations, each time resampling (with replacement) the set of observed ranks and weights.
454 This procedure yielded distributions of 100 estimated slopes for each experimental condition. We
455 used these distributions to compare the slopes across experimental conditions and to estimate 95%
456 confidence intervals.

457 Synthetic data

458 To help illustrate the relationship between informativeness and compressibility (Fig. 1), we gen-
459 erated four synthetic datasets, varying in informativeness and compressibility. Each dataset com-
460 prised simulated observations of $K = 25$ features across $N = 100$ timepoints, from each of $S = 10$
461 participants. To create each dataset, we first constructed a “template” matrix of N timepoints by K
462 features. We then generated participant-specific data by adding independent noise to each entry
463 in template matrix, drawn from the unit normal distribution (i.e., with a mean of 0 and a variance
464 of 1). We repeated this process for each participant, yielding S participant-specific matrices for
465 each dataset.

466 Since we estimate informativeness using the temporal decoding accuracy across participants,
467 highly informative data will tend to have observations that are highly timepoint specific. Relatively
468 uninformative data, in contrast, will tend to have more similar observations across timepoints. To
469 generate data with “high informativeness,” we constructed template matrices whose rows (ob-
470 servations) were drawn independently from zero-mean multivariate normal distributions. The
471 covariances of these distributions were determined according to the desired compressibility of
472 the data, as described below. We used a multi-step process to generate data with “low informa-
473 tiveness.” First we generated new template matrices using the same procedure as for the “high

474 informativeness” datasets. We then multiplied each matrix by a constant ($\rho = 0.1$) and computed
475 the cumulative sum of each matrix’s rows. This yielded matrices whose rows were highly similar
476 across observations.

477 Compressibility reflects the extent to which decoding accuracy is affected by reducing the num-
478 ber of components used to represent the data. Highly compressible data will tend to exhibit more
479 similarities across features, whereas less compressible data will tend to show greater independence
480 across features. To generate data with “high compressibility,” we set the covariance matrix of the
481 multivariate normal distribution to a toeplitz matrix whose first row was given by $[K, K - 1, \dots, 1]$.
482 To generate data with “low compressibility,” we set the covariance matrix to the identity matrix.

483 Template matrices for datasets with high informativeness and high compressibility, high in-
484 formativeness and low compressibility, low informativeness and high compressibility, and low
485 informativeness and low compressibility are displayed in Figure 1C. The corresponding decoding
486 curves are displayed in Figure 1D.

487 **Data and code availability**

488 All of the code used to produce the figures and results in this manuscript, along with links to the
489 corresponding data, may be found at github.com/ContextLab/pca_paper.

490 **Acknowledgements**

491 We acknowledge discussions with Rick Betzel, Luke Chang, Emily Finn, and Jim Haxby. Our
492 work was supported in part by NSF CAREER Award Number 2145172 to J.R.M. The content is
493 solely the responsibility of the authors and does not necessarily represent the official views of our
494 supporting organizations. The funders had no role in study design, data collection and analysis,
495 decision to publish, or preparation of the manuscript.

496 **Author contributions**

497 Conceptualization: J.R.M. and L.L.W.O. Methodology: J.R.M. and L.L.W.O. Implementation:
498 J.R.M. and L.L.W.O. Analysis: J.R.M. and L.L.W.O. Writing, Reviewing, and Editing: J.R.M. and

499 L.L.W.O. Funding acquisition: J.R.M. Supervision: J.R.M.

500 **References**

- 501 Adachi, Y., Osada, T., Sporns, O., Watanabe, T., Matsui, T., Miyamoto, K., & Miyashita, Y.
502 (2012). Functional connectivity between anatomically unconnected areas is shaped by collective
503 network-level effects in the macaque cortex. *Cerebral Cortex*, 22(7), 1586–1592.
- 504 Alvarez, S. A. (2002). *An exact analytical relation among recall, precision, and classification accuracy in*
505 *information retrieval* (Technical Report No. BCCS-02-01). Boston College.
- 506 Baldassano, C., Chen, J., Zadbood, A., Pillow, J. W., Hasson, U., & Norman, K. A. (2017). Discov-
507 ering event structure in continuous narrative perception and memory. *Neuron*, 95(3), 709–721.
- 508 Bassett, D. S., & Sporns, O. (2017). Network neuroscience. *Nature Neuroscience*, 20(3), 353–364.
- 509 Benjamini, Y., & Hochberg, Y. (1995). Controlling the False Discovery Rate: a practical and
510 powerful approach to multiple testing. *Journal of Royal Statistical Society, Series B*, 57, 289–300.
- 511 Blei, D. M., Ng, A. Y., & Jordan, M. I. (2003). Latent dirichlet allocation. *Journal of Machine Learning*
512 *Research*, 3, 993–1022.
- 513 Brovelli, A., Ding, M., Ledberg, A., Chen, Y., Nakamura, R., & Bressler, S. (2004). Beta oscillations in
514 a large-scale sensorimotor cortical network: directional influences revealed by Granger causality.
515 *Proceedings of the National Academy of Sciences, USA*, 101(26), 9849–9854.
- 516 Bullmore, E., & Sporns, O. (2009). Complex brain networks: graph theoretical analysis of structural
517 and functional systems. *Nature Reviews Neuroscience*, 10(3), 186–198.
- 518 Capota, M., Turek, J., Chen, P.-H., Zhu, X., Manning, J. R., Sundaram, N., ... Shin, Y. S. (2017).
519 *Brain imaging analysis kit*.
- 520 Chen, P.-H. A., Jolly, E., Cheong, J. H., & Chang, L. J. (2020). Intersubject representational
521 similarity analysis reveals individual variations in affective experience when watching erotic
522 movies. *NeuroImage*, 216(116851), doi.org/10.1016/j.neuroimage.2020.116851.

- 523 Cole, M. W., Bassett, D. S., Power, J. D., Braver, T. S., & Petersen, S. E. (2014). Intrinsic and
524 task-evoked network architectures of the human brain. *Neuron*, 83(1), 238–251.
- 525 Dhamala, M., Rangarajan, G., & Ding, M. (2008). Analyzing information flow in brain networks
526 with nonparametric Granger causality. *NeuroImage*, 41(2), 354–362.
- 527 Finn, E. S., Scheinost, D., Finn, D. M., Shen, X., Papademetris, X., & Constable, R. T. (2017).
528 Can brain state be manipulated to emphasize individual differences in functional connectivity.
529 *NeuroImage*, 160, 140–151.
- 530 Finn, E. S., Shen, X., Scheinost, D., Rosenberg, M. D., Huang, J., Chun, M. M., ... Constable, R. T.
531 (2015). Functional connectome fingerprinting: identifying individuals using patterns of brain
532 connectivity. *Nature Neuroscience*, 18, 1664–1671.
- 533 Fox, A. S., Chang, L. J., Gorgolewski, K. J., & Yarkoni, T. (2014). Bridging psychology and
534 genetics using large-scale spatial analysis of neuroimaging and neurogenetic data. *bioRxiv*,
535 doi.org/10.1101/012310.
- 536 Glerean, E., Salmi, J., Lahnakoski, J. M., Jääskeläinen, I. P., & Sams, M. (2012). Functional magnetic
537 resonance imaging phase synchronization as a measure of dynamic functional connectivity.
538 *Brain Connectivity*, 2(2), 91–101.
- 539 Gratton, C., Laumann, T. O., Nielsen, A. N., Greene, D. J., Gordon, E. M., Gilmore, A. W., ...
540 Petersen, S. E. (2018). Functional brain networks are dominated by stable group and individual
541 factors, not cognitive or daily variation. *Neuron*, 98(2), 439–452.
- 542 Hasson, U., Yang, E., Vallines, I., Heeger, D. J., & Rubin, N. (2008). A hierarchy of temporal
543 receptive windows in human cortex. *The Journal of Neuroscience*, 28(10), 2539–2550.
- 544 Korzeniewska, A., Crainiceanu, C. M., Kus, R., Franaszczuk, P. J., & Crone, N. E. (2008). Dynamics
545 of event-related causality in brain electrical activity. *Human Brain Mapping*, 29(10).
- 546 Kumar, M., Anderson, M. J., Antony, J. W., Baldassano, C., Brooks, P. P., Cai, M. B., ... Norman,
547 K. A. (2021). BrainIAK: the brain image analysis kit. *Aperture*, *In press*.

- 548 Lerner, Y., Honey, C. J., Silbert, L. J., & Hasson, U. (2011). Topographic mapping of a hierarchy of
549 temporal receptive windows using a narrated story. *The Journal of Neuroscience*, 31(8), 2906–2915.
- 550 Lynn, C. W., & Bassett, D. S. (2021). Quantifying the compressibility of complex networks.
551 *Proceedings of the National Academy of Sciences, USA*, 118(32), e2023473118.
- 552 Mack, M. L., Preston, A. R., & Love, B. C. (2020). Ventromedial prefrontal cortex compression during
553 concept learning. *Nature Communications*, 11(46), doi.org/10.1038/s41467-019-13930-8.
- 554 Manning, J. R. (2020). Context reinstatement. In M. J. Kahana & A. D. Wagner (Eds.), *Handbook of
555 human memory*. Oxford University Press.
- 556 Manning, J. R., Zhu, X., Willke, T. L., Ranganath, R., Stachenfeld, K., Hasson, U., ... Norman,
557 K. A. (2018). A probabilistic approach to discovering dynamic full-brain functional connectivity
558 patterns. *NeuroImage*, 180, 243–252.
- 559 Norman, K. A., Polyn, S. M., Detre, G. J., & Haxby, J. V. (2006). Beyond mind-reading: multi-voxel
560 pattern analysis of fMRI data. *Trends in Cognitive Sciences*, 10(9), 424–430.
- 561 OpenAI. (2023, March). *ChatGPT*. Personal communication.
- 562 Owen, L. L. W., Chang, T. H., & Manning, J. R. (2021). High-level cognition during story listening is
563 reflected in high-order dynamic correlations in neural activity patterns. *Nature Communications*,
564 12(5728), doi.org/10.1038/s41467-021-25876-x.
- 565 Owen, L. L. W., Muntianu, T. A., Heusser, A. C., Daly, P., Scangos, K. W., & Manning, J. R. (2020). A
566 Gaussian process model of human electrocorticographic data. *Cerebral Cortex*, 30(10), 5333–5345.
- 567 Preti, M. G., Bolton, T. A. W., & Van De Ville, D. (2017). The dynamic functional connectome:
568 state-of-the-art and perspectives. *NeuroImage*, 160, 41–54.
- 569 Regev, M., Simony, E., Lee, K., Tan, K. M., Chen, J., & Hasson, U. (2018). Propagation of information
570 along the cortical hierarchy as a function of attention while reading and listening to stories.
571 *Cerebral Cortex*.
- 572 Rogers, B. P., Morgan, V. L., Newton, A. T., & Gore, J. C. (2007). Assessing functional connectivity
573 in the human brain by fMRI. *Magnetic Resonance Imaging*, 25(11), 1347–1357.

- 574 Rubin, T. N., Kyojo, O., Gorgolewski, K. J., Jones, M. N., Poldrack, R. A., & Yarkoni, T. (2017).
575 Decoding brain activity using a large-scale probabilistic functional-anatomical atlas of human
576 cognition. *PLoS Computational Biology*, 13(10), e1005649.
- 577 Rubinov, M., & Sporns, O. (2010). Complex network measures of brain connectivity: uses and
578 interpretations. *NeuroImage*, 52, 1059–1069.
- 579 Scangos, K. W., Khambhati, A. N., Daly, P. M., Owen, L. L. W., Manning, J. R., Ambrose, J. B.,
580 ... Chang, E. F. (2021). Biomarkers of depression symptoms defined by direct intracranial
581 neurophysiology. *Frontiers in Human Neuroscience*, In press.
- 582 Shannon, C. E. (1948). A mathematical theory of communication. *Bell System Technical Journal*,
583 27(3), 379–423.
- 584 Simony, E., & Chang, C. (2020). Analysis of stimulus-induced brain dynamics during naturalistic
585 paradigms. *NeuroImage*, 216, 116461.
- 586 Simony, E., Honey, C. J., Chen, J., & Hasson, U. (2016). Dynamic reconfiguration of the default
587 mode network during narrative comprehension. *Nature Communications*, 7(12141), 1–13.
- 588 Sizemore, A. E., Giusti, C., Kahn, A., Vettel, J. M., Betzel, R. F., & Bassett, D. S. (2018). Cliques and
589 cavities in the human connectome. *Journal of Computational Neuroscience*, 44(1), 115–145.
- 590 Smith, S. M., Beckmann, C. F., Andersson, J., Auerbach, E. J., Bijsterbosch, J., Douaud, G., ...
591 Glasser, M. F. (2013). Resting-state fMRI in the Human Connectome Project. *NeuroImage*, 80,
592 144–168.
- 593 Smith, S. M., Fox, P. T., Miller, K. L., Glahn, D. C., Fox, P. M., Mackay, C. E., ... Beckmann,
594 C. F. (2009). Correspondence of the brain's functional architecture during activation and rest.
595 *Proceedings of the National Academy of Sciences, USA*, 106(31), 13040–13045.
- 596 Smith, S. M., Hyvärinen, A., Varoquaux, G., Miller, K. L., & Beckmann, C. F. (2014). Group-PCA
597 for very large fMRI datasets. *NeuroImage*, 101, 738–749.

- 598 Smith, S. M., Vidaurre, D., Beckmann, C. F., Glasser, M. F., Jenkinson, M., Miller, K. L., ... Van
599 Essen, D. C. (2013). Functional connectomics from resting-state fMRI. *Trends in Cognitive Sciences*,
600 17(12), 666–682.
- 601 Sporns, O., & Betzel, R. F. (2016). Modular brain networks. *Annual Review of Psychology*, 67,
602 613–640.
- 603 Sporns, O., & Honey, C. J. (2006). Small worlds inside big brains. *Proceedings of the National Academy
of Sciences, USA*, 103(51), 19219–19220.
- 605 Sporns, O., & Zwi, J. D. (2004). The small world of the cerebral cortex. *Neuroinformatics*, 2(2),
606 145–162.
- 607 Srinivasan, R., Winter, W. R., Ding, J., & Nunez, P. L. (2007). EEG and MEG coherence: Measures of
608 functional connectivity at distinct spatial scales of neocortical dynamics. *Journal of Neuroscience
Methods*, 166, 41–52.
- 610 Sul, S., Güroğlu, B., Crone, E. A., & Chang, L. J. (2017). Medial prefrontal cortical thinning
611 mediates shifts in other-regarding preferences during adolescence. *Scientific Reports*, 7(8510),
612 doi.org/10.1038/s41598-017-08692-6.
- 613 Tomasi, D., & Volkow, N. D. (2011). Association between functional connectivity hubs and brain
614 networks. *Cerebral Cortex*, 21, 2003–2013.
- 615 Yeo, B. T. T., Krienen, F. M., Sepulcre, J., Sabuncu, M. R., Lashkari, D., Hollinshead, M., ... Buckner,
616 R. L. (2011). The organization of the human cerebral cortex estimated by intrinsic functional
617 connectivity. *Journal of Neurophysiology*, 106(3), 1125–1165.